Agricultural Water Management 260 (2022) 107320

Contents lists available at ScienceDirect

Agricultural Water Management

journal homepage: www.elsevier.com/locate/agwat

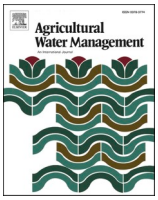

A remote sensing and modeling integrated approach for constructing continuous time series of daily actual evapotranspiration

Hassan Awada [a,*], Simone Di Prima [a], Costantino Sirca [a,b], Filippo Giadrossich [a], Serena Marras [a,b], Donatella Spano [a,b], Mario Pirastru [a]

[a] Department of Agricultural Sciences, University of Sassari, Viale Italia 39, 07100 Sassari, Italy
[b] Euro-Mediterranean Centre on Climate Change (CMCC) Foundation, Via de Nicola 9, 07100 Sassari, Italy

ARTICLE INFO

Handling Editor: Xiying Zhang

Keywords:
Surface energy balance
Evaporation
Transpiration
NDVI
Soil moisture
Eddy covariance

ABSTRACT

Satellite remote sensing-based surface energy balance (SEB) techniques have emerged as useful tools for quantifying spatialized actual evapotranspiration at various temporal and spatial scales. However, discontinuous data acquisitions and/or gaps in image acquisition due to cloud cover can limit the applicability of satellite remote sensing (RS) in agriculture water management where continuous time series of daily crop actual evapotranspiration ($ET_{c\ act}$) are more valued. The aim of the research is to construct continuous time series of daily $ET_{c\ act}$ starting from temporal estimates of actual evapotranspiration obtained by SEB modelling ($ET_{a\ eb}$) on Landsat-TM images. SEBAL model was integrated with the FAO 56 evaporation model, RS-retrieved vegetative biomass dynamics (by NDVI) and on-field measurements of soil moisture and potential evapotranspiration. The procedure was validated by an eddy covariance tower on a vineyard with partial soil coverage in the south of Sardinia Island, Italy. The integrated modeling approach showed a good reproduction of the time series dynamics of observed $ET_{c\ act}$ (R^2 =0.71, MAE=0.54 mm d^{-1}, RMSE=0.73 mm d^{-1}). A daily and a cumulative monthly temporal analysis showed the importance of integrating parameters that capture changes in the soil-plant-atmosphere (SPA) continuum between Landsat acquisitions. The comparison with daily $ET_{c\ act}$ obtained by the referenced ET fraction (ET_{rF}) method that considers only weather variability (by ET_o) confirmed the lead of the proposed procedure in the spring/early summer periods when vegetation biomass changes and soil water evaporation have a significant weight in the ET process. The applied modelling approach was also robust in constructing the missing $ET_{c\ act}$ data under scenarios of limited cloud-free Landsat acquisitions. The presented integrated approach has a great potential for the near real time monitoring and scheduling of irrigation practices. Further testing of this approach with diverse dataset and the integration with the soil water modeling is to be analyzed in future work.

1. Introduction

Evapotranspiration (ET) in arid and semi-arid environments is a major component of the hydrological cycle and one of the most important physical processes of the land-surface. In agriculture, quantifying the spatial variability and the temporal dynamic of ET at the field or larger spatial scales is of great importance for irrigation scheduling, identifying water productivity and water use efficiency (Molden et al., 2010; Stanhill, 1986). These activities are particularly relevant in the modern precision agriculture applications. Over large areas, such as irrigation districts or basins, time series of spatialized evapotranspiration data serve for assessing crop water requirements for adapting collective irrigation schemes, and for planning an optimal allocation of water resources. In the coming years with the reduced availability of natural water resources and increased water consumption in agriculture (Masia et al., 2021), recursively updated ET maps will serve for designing or validating strategies of adaptation to climatic changes.

Local measurements of evapotranspiration, such as lysimeters or micrometeorological methods (i.e., Bowen Ratio, Eddy Covariance and Scintillometers) have proven to be reliable to measure crop actual evapotranspiration and can be considered as the references against which spatialized $ET_{c\ act}$ estimation methods could be validated. However, local measurements are considered labor and cost-intensive (Droogers et al., 2000; Elhaddad and Garcia, 2008) and are rarely

* Corresponding author.
E-mail address: hassan_awada1987@live.com (H. Awada).

https://doi.org/10.1016/j.agwat.2021.107320
Received 20 July 2021; Received in revised form 25 October 2021; Accepted 1 November 2021
Available online 15 November 2021

available worldwide (Ochoa-Sánchez et al., 2019). The spatial extrapolation or interpolation of local $ET_{c\ act}$ measurements over larger spatial scales is problematic; moreover, it cannot be representative of land cover and/or management practices diverse from those of the measurement site. In this context, comes the need to find reliable and non-expensive alternative procedures capable of quantifying the spatial variability of $ET_{c\ act}$, both on the field and at larger spatial scales. This issue directed part of the scientific research towards developing and fine-tuning of mathematical models capable of providing a detailed description of mass and energy exchange processes in the soil-plant-atmosphere (SPA) continuum. In parallel, a significant effort was given to integrating modeling and observations from satellite or aerial platforms with the scope of computing spatialized $ET_{c\ act}$ values.

Low-cost remote sensing techniques can be used to retrieve the space-time variability of numerous physical variables needed in the applications of the $ET_{c\ act}$ modeling (Bastiaanssen et al., 2000; D'Urso, 2001; Kustas et al., 2003; Menenti, 2000; Morse et al., 2000). For example, mathematical modeling based on the application of hydrological balance in the SPA system can benefit from data operating in the visible and near-infrared (VIS/NIR regions of the electromagnetic spectrum) for the retrieval of the biophysical properties of the vegetation cover (D'Urso, 2001; Consoli and Vanella, 2014). On the other hand, surface energy balance (SEB) based approaches can use, in addition to the data acquired in the VIS and NIR regions, those acquired in the thermal infrared (TIR) for the estimation of $ET_{a\ eb}$ as a residual of the SEB equation, after quantifying the rest of the instantaneous fluxes (Gowda et al., 2008; Wagle et al., 2017; Bhattarai et al., 2016; Maltese et al., 2018; Minacapilli et al., 2016). SEB models like SEBAL (Bastiaanssen et al., 1998a), SEBS (Su, 2002) and METRIC (Allen et al., 2007) are single source SEB models that treat a pixel as a single transfer layer (Wagle et al., 2017). Other dual source SEB based models such as TSEB (Norman et al., 1995) and the STSEB (Häusler et al., 2018) parametrize and differentiate between the radiative and convective exchange processes between soil and vegetation and the atmosphere (Timmermans et al., 2007). Satellite-based SEB models have been applied and validated extensively in various parts of the world (Awada et al., 2021; Allen et al., 2007; Bastiaanssen et al., 1998b; Bhattarai et al., 2016; Maltese et al., 2018; Timmermans et al., 2007). Such modelling approaches has been widely applied in irrigation management (Allen et al., 2007; Bastiaanssen et al., 2001, 1996; Senay et al., 2017), water accounting (Molden and Sakthivadivel, 1999), assessing irrigation system performance (Akbari et al., 2007; Al Zayed et al., 2015; Awada et al., 2019), agricultural water productivity (Blatchford et al., 2018; Zwart et al., 2010), groundwater management (Ahmad et al., 2005, 2014; Rodell et al., 2009), and hydrological modelling (Cammalleri et al., 2010; Droogers and Bastiaanssen, 2002; Immerzeel and Droogers, 2008; Muthuwatta et al., 2010). Satellite-based SEB approaches can capture large geographical extents and provide $ET_{a\ eb}$ estimations at different spatial and temporal scales; however, some limitations to the use of the satellite images still exist due to the platform's spatial resolutions, revisit times and the cloudiness at the overpass times. For example, the AATSR/ENVISAT, the MODIS and the Sentinel-3 satellites have a short revisit time (1 day) but a 1000 m spatial resolution of the thermal infrared. The use of these data in $ET_{a\ eb}$ modelling is limited to the spatial extent of the TIR data and is not recommended in fragmented and heterogeneous agriculture, especially when the parcels are smaller than the TIR pixel. Alternatively, relatively high spatial resolution TIR imagery (from 60 to 120 m) can be obtained from platforms such as Landsat and ASTER, however, images are available every 16 days, if clear sky condition exists at the overpass time. McCabe and Wood (2006) found a high degree of consistency of $ET_{a\ eb}$ retrievals from Landsat and ASTER and showed that low spatial resolution MODIS-based estimates were unable to discriminate the influence of land surface heterogeneity at the field spatial scale. The Ecosystem Spaceborne Thermal Radiometer Experiment on Space Station (ECOSTRESS) recently launched measures TIR data along an irregular non-polar orbit at a ~70 m spatial resolution and an overpass time of 1–5 days. This represents a significant improvement in terms of temporal sampling of land surface temperature (LST) required to derive reliable $ET_{a\ eb}$ products at the field scale, however ECOSTRESS is a thermal-only experimental sensor, it does not provide data for high latitudes and its use in SEB modeling is dependent on VSWIR (visible to shortwave infrared bands) data from other platforms.

For agricultural applications, e.g., irrigation scheduling or water resources management, $ET_{c\ act}$ values are required on a daily basis, over extended periods (e.g. irrigation season, Allen et al., 2007) and with a fine spatial scale (e.g. Agricultural field). Several approaches have been proposed to produce continuous data series of daily $ET_{c\ act}$ at the field scale by using remote sensing techniques. Bisquert et al. (2016) and Kustas et al. (2003) applied disaggregation techniques to downscale the TIR data of MODIS to the spatial resolution of VIS/NIR of SPOT 5 (10 m spatial resolution and 5-day revisit time). Other researchers downscaled the TIR data from low resolution sensors (MODIS, AATSR or Sentinel-3) to the spatial scale of medium-high resolution sensors (ASTER, Landsat) (Bindhu et al., 2013; Bisquert et al., 2016; Olivera-Guerra et al., 2017). Besides disaggregation techniques, data fusion methods are based on the spectral and spatial relationship between an existing high/low-resolution image pair (Cammalleri et al., 2013; Gao et al., 2006; Semmens et al., 2016; Bhattarai et al., 2014; Ma et al., 2018). This relationship is used to realize high spatial resolution data for dates when only the low-resolution images are available (Bisquert et al., 2016). However, methods that fuse intermediate variables directly related to the evapotranspiration process (Vegetation Indices, VI, and LST) are subject to several limitations. Indeed, remote sensing parameters (e.g., bit parameters, bandwidth, acquisition time, and spectral response function) acquired from different satellite sensors on the same date may not provide comparable data (Ma et al., 2018). Another limitation is that RS platforms used in these approaches have different acquisition times during the day. Furthermore, modeling the dynamics of these intermediate variables used in $ET_{c\ act}$ retrieval can add uncertainties.

Differently from the above-mentioned approaches, which integrate data from different platforms, other authors (Awada et al., 2019; Allen et al., 2007; Alfieri et al., 2017; Singh et al., 2012; Trezza et al., 2013) used the daily actual crop coefficient as a reference to construct the continuous times series of daily $ET_{c\ act}$ starting from $ET_{a\ eb}$ determined by RS-SEB models in cloud-free image acquisition days. Precisely, a so-called referenced ET fraction, ET_{rF} (unitless), is computed as $ET_{a\ eb}/ET_o$ on the image acquisition days and used together with the daily changes of daily reference crop evapotranspiration (ET_o), continuously monitored in a weather station, to drive the $ET_{c\ act}$ changes in the other days. In the $ET_{c\ act}$ construction period between the acquisition days the ET_{rF} is kept constant or is changed by interpolation. Using this daily $ET_{c\ act}$ construction approach, some authors considered that typically one or two cloud-free Landsat images are considered enough to derive monthly $ET_{c\ act}$ (Allen et al., 2007; Bhattarai et al., 2012). Conversely, Trezza et al. (2018) considered that the estimation error in monthly $ET_{c\ act}$ is relatively high when image availability is limited to an eight-day revisit time satellite data and suggested a four-day revisit time to robustly represent time-integrated $ET_{c\ act}$ estimates over months and growing seasons. Alfieri et al. (2017) assessed daily $ET_{c\ act}$ estimations derived using different temporal autocorrelation reference variables, including the ET_o, and interpolation methods. They found that a return interval of earth observations of a minimum of five days is necessary to estimate daily $ET_{c\ act}$ with relative errors smaller than 20%. Moreover, constructing the time series of daily $ET_{c\ act}$ by the ET_{rF} approach considers the variability of the meteorological inputs (embedded in the daily ET_o). Still, it cannot account for the effect of soil moisture dynamics (due to precipitation, irrigation, and $ET_{c\ act}$), plant stress, and/or the vegetation biomass changes (i.e., crop development, cuttings in case of forage crops) that occur between images acquisitions. Besides, methods involving the linear or cubic spline interpolation of ET_{rF} (Allen et al., 2007; Singh et al., 2012) limit the applicability for near real-time

modelling of daily $ET_{c\ act}$.

This paper proposes a simple integrated model-based procedure to construct the daily $ET_{c\ act}$ data between satellite image acquisition days. The dynamics of meteorological variables, vegetation biomass changes and/or plant stress caused by soil water restriction drive the $ET_{c\ act}$ changes between different acquisitions. To estimate $ET_{a\ eb}$ on image acquisition days we applied the Surface Energy Balance Algorithm for Land (SEBAL) model (Bastiaanssen et al., 1998a), The model was selected, because of its relative simplicity and low requirement for ancillary data, moreover it was extensively applied and validated over a range of environmental conditions and vegetation types (Awada et al., 2021; Bastiaanssen et al., 2002, 2005, 1998b; Li and Zhao, 2010; Zwart and Bastiaanssen, 2007). SEBAL was applied with Landsat 5 Thematic Mapper (TM) images and limited meteorological inputs. The integrated $ET_{c\ act}$ construction procedure was tested over a vineyard with partial soil coverage in the south of Sardinia Island, Italy. The $ET_{c\ act}$ construction approach combines the daily values of ET_o, remotely sensed vegetation indices, observed soil moisture in the root zone, and a modeling approach for the soil water evaporation.

Specifically, the research was carried out with the following objectives:

i. constructing a continuous time series of daily $ET_{c\ act}$ values for the vegetation period of a vineyard starting from few $ET_{a\ eb}$ data estimated by SEBAL, daily ET_o, NDVI from satellite and on-field observed soil moisture;
ii. evaluating the performance of the proposed methodology by comparison with in-situ Eddy-covariance (EC) flux measurements.

2. The core structure of the daily $ET_{c\ act}$ construction procedure

To obtain the continuous time-series of daily $ET_{c\ act}$, the actual evapotranspiration obtained by a SEB model on acquisition days is integrated with an $ET_{c\ act}$ construction modelling procedure. This latter accounts for the temporal dynamics of daily ET_o, satellite-derived vegetation indices, soil moisture data and includes a water balance modelling approach for the estimation of canopy water interception and soil water evaporation. Thus, the procedure accounts for changes in daily weather, vegetative biomass and plant water stress that occur between the TIR satellite data acquisitions.

The proposed $ET_{c\ act}$ construction approach computes separately the daily actual values of canopy water interception, I_c, soil water evaporation, E_s, and crop actual transpiration, $T_{c\ act}$. The canopy water interception and soil water evaporation are modeled on an hourly time scale (see Sections 3.6 and 3.8). In images acquisition days the transpiration, $T_{c\ act,A.D}$, is obtained by subtracting the daily values of canopy water interception, $I_{c,A.D.}$ and soil water evaporation, $E_{s,A.D.}$, from the SEB retrieved actual evapotranspiration value, $ET_{a\ eb}$ (Eq. 1). In the other days (indicated by j subscript in equations below) the actual crop transpiration values are computed by Eq. (2), assuming proportionality among $T_{c\ act,A.D}$ and the changes of ET_o, NDVI and crop water stress coefficients (K_s) between the acquisition day and the other days j. K_s is obtained based on soil moisture in the plant root zone (Section 3.7). Eq. (2) is applied forwardly starting from each one of the acquisition days. The daily actual evapotranspiration in non-acquisition days, $ET_{c\ act,j}$ is the sum of the modeled daily crop actual transpiration ($T_{c\ act,j}$),the canopy water interception ($I_{c,j}$) and the soil water evaporation ($E_{s,j}$).

$$T_{c\ act,A.D.} = ET_{a\ eb} - E_{s,A.D.} - I_{c,A.D.} \quad (1)$$

$$T_{c\ act,j} = T_{c\ act,A.D.} \cdot \frac{ET_{o,j}}{ET_{o,A.D.}} \cdot \frac{NDVI_j}{NDVI_{A.D.}} \cdot \frac{K_{s,j}}{K_{s,A.D.}} \quad (2)$$

$$ET_{c\ act,j} = E_{s,j} + I_{c,j} + T_{c\ act,j} \quad (3)$$

The daily $ET_{c\ act}$ construction procedure integrated with the SEBAL model is outlined in the flowchart of Fig. 1.

3. Materials and methods

3.1. Case study

The experimental site is located within the Argiolas company

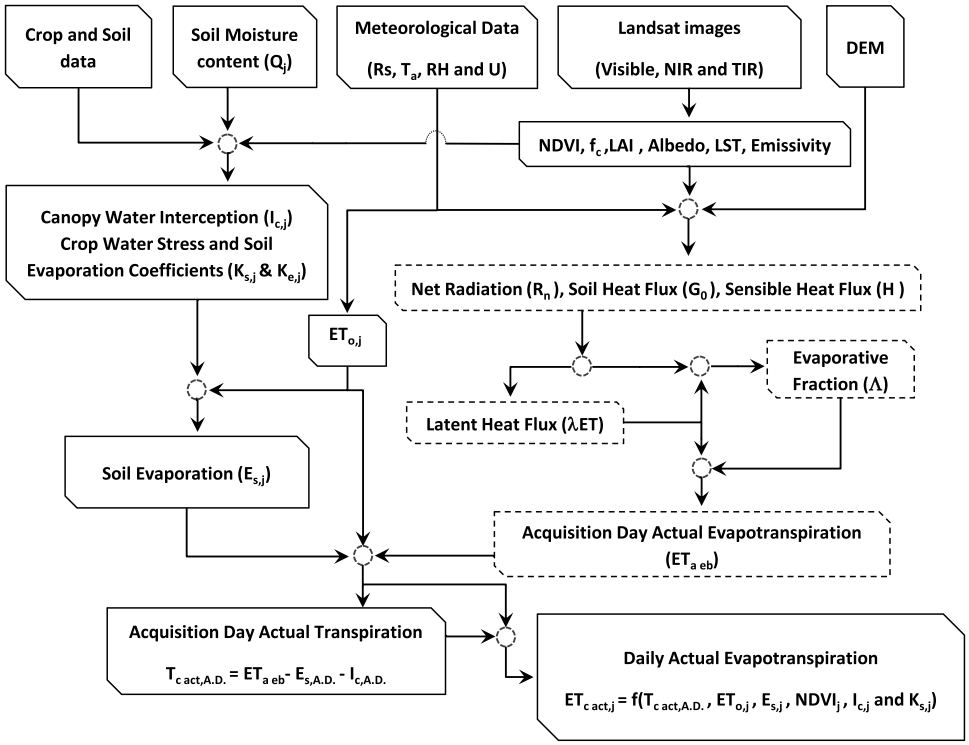

Fig. 1. Flowchart of integrated SEBAL-daily $ET_{c\ act}$ construction procedure (*SEBAL outputs are highlighted as dashed polygons).

vineyards near Serdiana municipality in Sardinia Island, Italy (39°21'43'' N, 9°07'26'' E, 112 m a.s.l., Fig. 2). The area is characterized by the semi-arid Mediterranean climate, with a warm summer, mild winter, and a high-water deficit from May through September. The mean precipitation is 484 mm yr^{-1}, mainly concentrated from autumn to spring. The mean annual temperature is 16.9 °C. The studied field is an 11-hectares Vermentino variety vineyard, trained in a Guyot system and oriented in east-west rows with 0.8 m between plants and 2.0 m between rows. The vegetation is about 2.0 m tall with about 50% ground shading at the maximum of the plant development at the end of July. In the inter-row spacing a minimal tillage is applied in order to prevent competitive vegetation growth. Vine roots were mostly concentrated in the first soil layers (0–0.6 m) of the row spacing, and some roots were found at more than 1 m of depth. Soil texture is a silty clay loam with 46% sand, 27% silt, 27% clay, soil field capacity (θ_{FC}) of 27.4% vol vol^{-1}, and a wilting point of 13.8% vol vol^{-1} and a basic pH (Mameli et al., 2012). The precipitation volume during the study period (form 21st April to the 6th of November) was 219 mm. Drip irrigation is performed during the dry summer seasons. Dripper lines were located in the vine rows, and drippers were placed close to the plants, one for plant, determining a partial overlapping of the wet bulbs along the vine rows. According to local production practices, the water is applied with the application of 14 mm of water every 5–7 days during the no-rainfall periods (Marras et al., 2016).

3.2. Micrometeorological measurements and data processing

An Eddy Covariance (EC) station (Fig. 1) was set up in 2009 to continuously monitor energy and mass fluxes (Marras et al., 2016). The EC system consisted of an IRGA Li-7500 open-path gas infrared analyzer (Li-Cor Biosciences, Lincoln, NE, USA), a CSAT3 three-dimensional sonic anemometer and a CR5000 datalogger (Campbell Scientific, Logan, UT, USA). Instruments were set up at 2.8 m above the ground, and the studied vineyard is located on a flat surface surrounded by other vineyards. The instrumentation height was decided after preliminary footprint analysis. The minimum distance from the end of the canopy is 150 m, and the footprint analysis carried out during all the measurements period confirmed that we were sampling the vineyard canopy. The fetch was estimated at about 500 m in all directions as reported in Marras et al. (2016). Instrument positioning was also the result of several years of experience measuring Eddy fluxes over vineyards, indicating that fluxes are not affected by the surface roughness. Data were acquired at 10 Hz, and covariances were calculated every 30 min. The station also measured the soil heat flux (G) by 4 heat flux plates (HFP01SC, Hukseflux, Delft, NL), installed in a transect between rows at 0.07 m of soil depth. Soil temperature changes in the soil above −0.07 m were measured by temperature probes placed above the soil heat flux plates close the top of the soil, to correct for heat storage and estimate G at the surface following the procedure in De Vries (1963). Terrestrial radiation (W m^{-2}) was also measured to determine net radiation (R_n) through a REBS Net Radiometer (Campbell Scientific Inc. (CSI), Logan, UT, USA). The software EddyPro v. 4.2.1 (Li-Cor Biosciences) was used to process raw data and perform the data quality check required by the international measurement protocol (Fluxnet network). In addition, a meteorological station was established near the vineyard to acquire every 30 min downward and upward short and long wave radiations, air temperature (T), relative air humidity (RH), precipitation (P), wind speed (u_2) and atmospheric pressure at 2 m above the ground. These data were used to run the SEBAL model and to compute the hourly and daily reference evapotranspiration (ET_o) by the Penman-Monteith method.

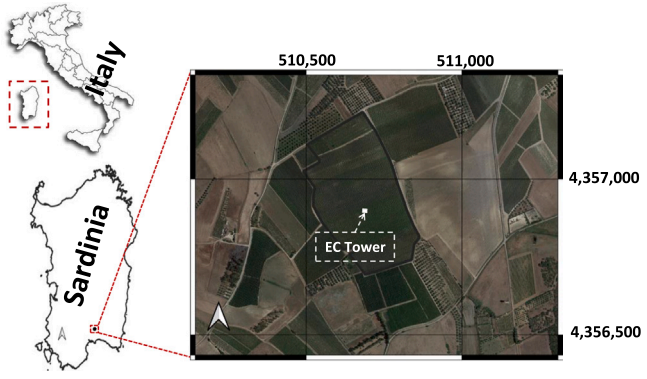

Fig. 2. Geographic location of the vineyard and the Eddy Covariance (EC) station. Coordinates EPSG:32632 (WGS 84 / UTM zone 32 N).

Marras et al. (2016) evaluated the energy balance closure during the years 2009 and 2010 by comparing the available energy (R_n-G) to the turbulent fluxes, that is the sum of latent (λET) and sensible (H) heat fluxes. The average observed energy balance closure was 87% and the coefficient of determination R^2 was 0.9. A discrepancy between 20% and 30% from the ideal 100% closure is commonly observed in surface energy budget measurements (Wilson et al., 2002). Allen et al. (2011) considered that measurements with ± 15% energy budget closure error are reliable.

In this paper, the studied period was restricted from April to November 2010, which was the period from the bud break to the harvesting of the vineyard. The measured fluxes were corrected by forcing the energy closure using the Bowen ratio. Half-hour data quality was evaluated by the energy balance closure (C_R) by rationing available energy to the turbulent flux components (Wilson et al., 2002). Prueger et al. (2005) suggested that C_R was assessed for R_n greater than 100 W m^{-2}. The half-hour energy budget closure was considered satisfactory when $C_R > 0.85$ (Prueger et al., 2005; Wilson et al., 2002). For lesser C_R the energy budget closure was forced by attributing R_n-G to H and λET with the preservation of the Bowen ratio (β), defined as H/λET (Prueger et al., 2005) as follows:

$$\lambda ET_c = \frac{(R_n - G)}{(1+\beta)} \quad (4)$$

$$H_c = \beta \frac{(R_n - G)}{(1+\beta)} \quad (5)$$

where λET_c and H_c are the corrected values of the latent and sensible heat fluxes, respectively.

Half-hourly λET_c were summed to obtain daily latent heat flux densities (MJ m^{-2} d^{-1}), and converted to daily actual evapotranspiration values ($ET_{c\ act\ EC}$, mm d^{-1}).

The $ET_{c\ act\ EC}$ values were used as a reference for evaluating the performance of the integrated $ET_{c\ act}$ construction model. The model results were considered acceptable if the differences between simulated and observed actual crop evapotranspiration values were in range of commonly observed eddy covariance SEB closure errors, ± 20 as reported by Wilson et al. (2002). Model results with errors less than ± 15% were considered good estimations in reference to reliable eddy covariance SEB measurements (Allen et al., 2011).

3.3. Soil moisture monitoring

Marras et al. (2016) reported soil volumetric water content (θ) measured by TDR (Campbell Scientific Inc. CS615 Water Content Reflectometer) probes at 0.20, 0.40 and 0.60 m of soil depth, placed at three locations within the vineyard both in the vine root zone, between two drippers, and in the middle of the inter-row. In this study we considered only the probes on the vine's rows as representative of the soil moisture in the root zone. Fig. 2 shows averaged soil moisture contents monitored at the three soil depths in the root zone during the year 2010. Based on soil field capacity (FC) and wilting point values, leaf

gas exchanges and stem water potential collected in the same vineyard during 2009 and 2010 (Fernandes De Oliveira et al., 2013; Mameli et al., 2012), Marras et al. (2016) selected a θ value of 0.22 as a threshold to indicate well-watered conditions for plants (80% of FC). Data when $\theta < 0.22$ only occurred starting from late August (Fig. 3).

3.4. Landsat satellite datasets and processing

Twelve Landsat 5 Thematic Mapper (TM) images, cloud-free on the area of interest, were selected to cover the period from April to November 2010 (Table 1). Images and metadata were downloaded from the https://earthexplorer.usgs.gov/ web site, last accessed on the 25th of February 2021. The visible, near-infrared, mid-infrared, and short-wave-infrared (TM bands 1–5 and 7) are obtained at 30 m spatial resolution. The thermal infrared (TM 6th band) is acquired at 120 m spatial resolution and resampled by the data providers using the cubic convolution method to a 30 m pixel size. Landsat image subsets were created and processed to obtain surface reflectance and surface radiometric temperature for the area of interest.

The NDVI is obtained from the Landsat near-infrared (ρ_{NIR}) and the red (ρ_{Red}) spectral reflectance data (TM bands 4 and 3) as ρ_{NIR}- ρ_{Red} / ρ_{NIR}+ ρ_{Red} (Rouse et al., 1974). NDVI at the selected acquisition days were obtained as mean values over the studied field. For the j days the NDVI values were estimated by linear interpolation between the Landsat acquisition days.

3.5. The surface energy balance algorithm for land (SEBAL) model

The single source SEBAL model simulates the radiative and turbulent fluxes within an image pixel without differentiating between the different pixel components, that is the model schematizes soil–vegetation as a sole resistance layer (Bastiaanssen, 2000; Bastiaanssen et al., 2005, 1998a; Minacapilli et al., 2009). SEBAL is a model with a strong physical basis and low requirement of ground-based ancillary data (Allen et al., 2011; Bastiaanssen et al., 2008). In addition to VIS and NIR data, SEBAL model requires surface radiometric temperature derived from thermal infrared radiation on a cloud-free image scene. The Landsat images, accompanied by a 10 m digital elevation model (DEM) (http://www.sardegnageoportale.it/, last accessed on the 21st of January 2021) and half-hourly meteorological inputs obtained from the meteorological station, were used to produce the SEBAL data layers (i.e., land surface temperature, surface albedo, NDVI, and surface emissivity). The SEBAL model first retrieves the instantaneous net surface radiation flux R_n (W m^{-2}) from Landsat and meteorological data as a balance of incoming and outgoing radiation fluxes (Bastiaanssen et al., 2005, 1998a). The instantaneous value of soil heat flux, G (W m^{-2}), is estimated from NDVI, surface radiometric temperature, surface albedo and, and R_n, as Bastiaanssen et al. (1998a) proposed. SEBAL estimates the sensible heat flux H (W m^{-2}) as function of the temperature gradient between two reference heights, near-surface and air that governs the transfer of heat (ΔT) and the aerodynamic resistance to heat transport (Bastiaanssen et al., 2005, 1998a). SEBAL then obtains the instantaneous latent heat flux λET (W m^{-2}) as a residual of the surface energy balance:

$$\lambda ET = R_n - G - H \quad (6)$$

The instantaneous λET at the satellite overpass time is upscaled to the daily actual evapotranspiration value using the evaporative fraction (Λ) as an integration parameter under the so-called self-preservation hypothesis (Shuttleworth et al., 1989; Brutsaert and Sugita, 1992; Cammalleri et al., 2012; Chávez et al., 2008; Crago, 1996; Maltese et al., 2013). The evaporative fraction is the ratio of λET to the available energy (R_n-G). The daily actual evapotranspiration on the image acquisition day, $ET_{a\ eb}$ (mm d^{-1}), is obtained as follows:

$$ET_{a\ eb.} = \Lambda \frac{R_{n24}}{\lambda \rho_w} \quad (7)$$

where R_{n24} (MJ m^{-2} d^{-1}) is the net daily radiation estimated by the

Table 1
Selected Landsat 5 TM images.

Image	Acquisition day (mm/dd/yyyy)	Day of year (DOY)	Acquisition time (Scene center) (hh:mm UTC)	Pass	Row	Cloud Cover (%)
01	04/21/2010	111	9:51	192	33	1
02	06/08/2010	159	9:50	192	33	0
03	06/24/2010	175	9:50	192	33	6
04	07/10/2010	191	9:50	192	33	0
05	07/17/2010	198	9:56	193	33	0
06	07/26/2010	207	9:50	192	33	28
07	08/11/2010	223	9:50	192	33	0
08	09/19/2010	262	9:56	193	33	17
09	09/28/2010	271	9:50	192	33	15
10	10/14/2010	287	9:50	192	33	38
11	10/21/2010	294	9:56	193	33	0
12	11/06/2010	310	9:56	193	33	2

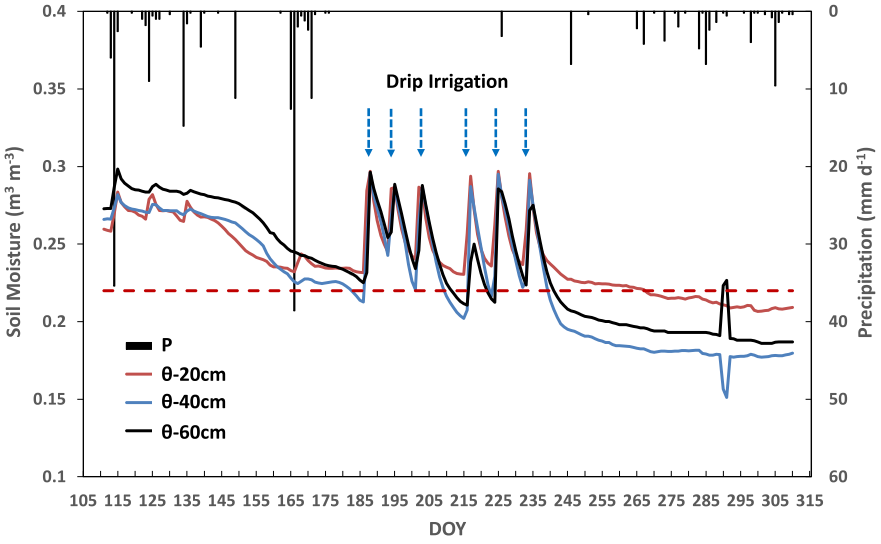

Fig. 3. Daily observed soil moisture (θ) at 0.2, 0.4 and 0.6 m of soil depth and precipitation (P). The dashed red line indicates the soil moisture threshold for plant stress. The dashed arrows indicate the drip irrigation applications.

procedure outlined in Allen et al. (1998).

The turbulent fluxes measured by the EC station change with the wind speed and direction. $ET_{a\ eb}$ was extracted by elliptical polygons (GIS shapefiles) that extend 100 m from the eddy covariance station and fall into line with the measured footprint orientation (upwind direction).

3.6. Canopy water interception

The actual canopy water interception (I_c) is modeled by an hourly water balance. The canopy water interception storage is filled by precipitation and is depleted by ET. When the I_c storage capacity (C) is reached, excess precipitation is generated and provides an input for the FAO-56 soil water evaporation model. C (mm) was determined from the Leaf Area Index (LAI) (Dickinson et al., 1991):

$$C = 0.2\,LAI \tag{8}$$

On the image acquisition days LAI was estimated by the Choudhury (1987) approach:

$$LAI = -\frac{\ln(1-fc)}{0.5} \tag{9}$$

where f_c is the fraction cover estimated on the image acquisition days from NDVI as proposed by Gutman and Ignatov (1998).

$$f_c = \frac{NDVI - NDVI_{min}}{NDVI_{max} - NDVI_{min}} \tag{10}$$

For the j days the f_c values were estimated by linear interpolation between each two Landsat acquisitions.

3.7. The stress index K_s

The crop water stress was simulated considering the observed soil moisture changes. The dimensionless weighed stress index (K_s) was derived from the relative water deficit in the different soil layers of the root zone (Jarvis, 1989). K_s was computed considering an effective root depth of 0.6 m. The soil moisture at each centimeter of the root zone (i = 0.01 m) was obtained by linear interpolation or extrapolation of the measured moisture data. The change of root water uptake as a function of the soil moisture was computed using a dimensionless plant water stress term

$$r_{s,i}(\theta) = \left\{ \begin{array}{cc} 1, & \theta_i \geq \theta_d \\ \frac{\theta_i - \theta_{WP}}{\theta_d - \theta_{WP}}, & \theta_i < \theta_d < \theta_{WP} \\ 0, & \theta_i \leq \theta_{WP} \end{array} \right\} \tag{11}$$

where θ_d is a moisture stress threshold, 80% of field capacity (about 60% of available water, Marras et al., 2016, Mameli et al., 2012) and θ_{WP} is the soil moisture at wilting point. In agreement with on field observations, it was assumed that plant roots are exponentially distributed with depth, such that:

$$\frac{r_{d,i}(z) = \Delta z \bullet \exp\left(-\frac{z_i}{L_{rd}}\right)}{L_{rd}} \tag{12}$$

where $r_{d,i}$ is the root mass fraction at the mid-point depth the soil layers i of thickness Δz= 0.01 m, L_{rd} is the depth above which 63% of plant root density is located, and is taken to be 0.3 m in line with field observation. Finally, the dimensionless weighed stress index K_s is calculated as:

$$K_s = \sum_{i=1}^{i=k} r_{s,i} r_{d,i} \tag{13}$$

where k is the total soil layer number (k = 60).

3.8. FAO-56 soil water evaporation model

The evaporation E_s for each day of the studied period, including the acquisition days, is obtained as:

$$E_s = K_e \cdot ET_o \tag{15}$$

where K_e is the daily soil evaporation coefficient, which is maximum when the topsoil is wet following a rain or irrigation and is zero when the topsoil is dry, and no water is available for evaporation. K_e is obtained following the FAO-56 dual crop coefficient approach (Allen et al., 1998):

$$K_e = K_r\left(K_{c,\ max} - K_{cb}\right) \leq f_{ew} \cdot K_{c,\ max} \tag{16}$$

where K_r is a dimensionless evaporation reduction coefficient, $K_{c,max}$ is the maximum value of K_c following a wetting event, K_{cb} is the basal crop coefficient, and f_{ew} is the fraction of the soil that is both exposed and wetted. The $f_{ew} \cdot K_{c,max}$ term restricts the evaporation by the energy available at the exposed soil fraction (Allen et al., 1998). The evaporation reduction coefficient K_r depends on the water depletion from the topsoil and is obtained on a daily basis:

$$K_r = \frac{TEW - D_e}{TEW - REW} \text{ if } D_e > REW \tag{17a}$$

$$K_r = 1 \text{ if } D_e \leq REW \tag{17b}$$

where D_e represents the actual cumulative depth of depletion from the soil surface layer and is computed by a soil water balance, TEW is the total evaporable water that represents the maximum cumulative depth of evaporation (depletion) from the soil surface layer, REW is the readily evaporable water, which represents the maximum depth of water that can evaporate from the topsoil layer without restriction. REW values were reported for the soil type in the FAO-56 paper, Table 19.

The total evaporable water is estimated from soil water content at field capacity, θ_{FC}, and at wilting point, θ_{WP}, for a depth Z_e (m) of the topsoil that is subject to drying by evaporation. Z_e was imposed equal to 0.1 m, accordingly with the values reported in the FAO-56 guidelines. It is assumed that the soil can dry to a water content level that is halfway between oven dry and wilting point (Allen et al., 1998).

$$TEW = 1000(\theta_{FC} - 0.5\theta_{WP})Z_e \tag{18}$$

The exposed and wetted soil fraction (f_{ew}) is obtained from the fractional vegetation cover (f_c) and the average fraction of soil surface wetted by irrigation or precipitation (f_w) as proposed in the FAO-56 approach (Allen et al., 1998).

$$f_{ew} = \min[f_0](1 - f_c,\quad [(1 - 2/3)f_c]f_w) \tag{19}$$

4. Results and discussion

4.1. Performance of the SEBAL model

The SEBAL model performance was evaluated at the image acquisition days in comparison with the on-field EC observations. This type of analysis is significant as the SEBAL performance influences the whole $ET_{c\ act,j}$ construction process. There was a good agreement between modeled $ET_{a\ eb}$ and observed $ET_{c\ act\ EC}$ (Fig. 4). The comparison yielded a coefficient of determination (R^2) of 0.96, and a mean absolute error (MAE) and root mean square error (RMSE) of 0.39 mm d^{-1} and 0.48 mm d^{-1}, respectively. Furthermore, a non-parametric Mann–Whitney test suggested no significant difference between the observed EC data and SEBAL estimations and that the null hypothesis can be accepted at significance level (α) of 0.05. Galleguillos et al. (2011) found a RMSE of 0.48 mm d^{-1} comparing the performance of the S-SEBI model estimates of daily evapotranspiration to EC observations over a Mediterranean vineyard and applied on 11 ASTER images. In another drip-irrigated

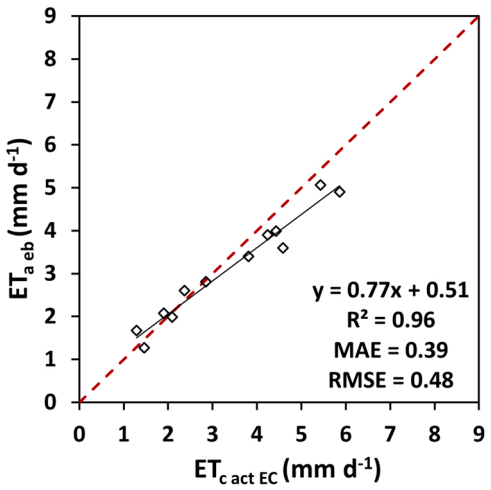

Fig. 4. Comparison of daily observed ($ET_{c\ act\ EC}$) and SEBAL modeled actual evapotranspiration ($ET_{a\ eb}$) on the Landsat image acquisition days (Table 1).

vineyard the METRIC model applied on 13 Landsat images overestimated the EC observed data with an average error of 9%, an RMSE of 0.62 mm $d^{-1}$and a MAE of 0.50 mm d^{-1} (Carrasco-Benavides et al., 2012). Knipper et al. (2019) applied the ALEXI/DisALEXI surface energy balance model with a large dataset of Landsat images over a vineyard and obtained an average estimation error of 15%, and a MAE and RMSE of 0.58 mm d^{-1} and 0.76 mm d^{-1}, respectively. The overall average SEBAL estimation error was 11.8%, the performance of the model on single days was within the error bounds of the state-of-the-art ET instruments (± 20%) except for $ET_{a\ eb}$ estimates on the 21st of April and 10th of July that overestimated the observed $ET_{c\ act\ EC}$ by 29% and 21%. These two acquisitions days fall in a period where the measured data SEB closure errors were exacerbated as observed by Marras et al. (2016), and therefore, the tendency to misestimate $ET_{c\ act\ EC}$ can be partly attributed to issues with the flux measurements closure and not the SEBAL model alone.

4.2. Performance of the integrated daily $ET_{c\ act}$ construction procedure

Fig. 5 compares the daily $ET_{c\ act}$ derived from the integrated construction procedure to the measured daily actual evapotranspiration ($ET_{c\ act\ EC}$) from the 21st of April (DOY 111) to the 6th of November

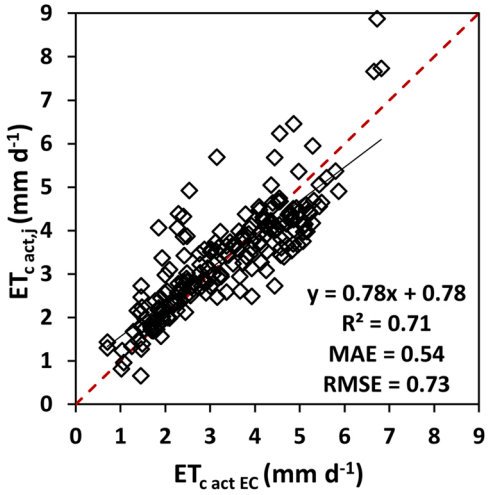

Fig. 5. Comparison of daily observed ($ET_{c\ act\ EC}$) and daily constructed crop actual evapotranspiration ($ET_{c\ act,j}$) on the studied period (21st of April to 6th of November 2010).

2010 (DOY 310). On average the modeled $ET_{c\ act}$ slightly underestimated the observed data. A non-parametric Mann–Whitney test suggested no significant difference between $ET_{c\ act}$ and $ET_{c\ act\ EC}$ at significance level (α) of 0.05. The average error of the $ET_{c\ act}$ estimations for the whole studied period was 18%. The comparison statistics (R^2 =0.71, MAE=0.54 mm d^{-1}, RMSE=0.73 mm d^{-1}) could be judged satisfactory considering that, in addition to SEBAL estimation errors and systematic eddy covariance energy balance closure uncertainties, the $ET_{c\ act,j}$ construction approach superimposes different kinds of simplifications. An example is the assumption of linearity between the crop water uptake, vegetation indices and crop water stress coefficients (Eq. 2). Such assumptions become less important as the time between acquisition days reduces, as for short time intervals also non-linear processes could be linearized with a sufficient degree of precision. Hence, the application of Eq. (2) potentially benefits from the relatively high availability of clear-sky image acquisitions, which could be provided by the upcoming capability of RS systems in capturing rapid changes even in the TIR domain (see Section 4.3 for further discussion). Moreover, several studies carried out in different areas supported a linear crop coefficient-VI relationships, (Beeri et al., 2019; Campos et al., 2010; Consoli and Vanella, 2014; Consoli and Barbagallo, 2012; O'Connell et al., 2011). In opposition, Er-Raki et al. (2013) used for a vineyard an exponential equation for fitting the experimental crop coefficient-VI relationship. However, also their relationship can be approximated by a linear regression without losing the goodness of fit. Furthermore, the direct proportionality of crop water uptake and water stress coefficients is at the basis of the K_S stress coefficient estimation in the FAO 56 approach for modelling actual crop evapotranspiration (Allen et al., 1998). The linearity between the crop water uptake, VIs and crop water stress coefficients was embedded in several modelling approaches and was sufficient for assessing actual ET_c for irrigation requirements in several crops, including vineyards and orchards (Campos et al., 2010; Consoli and Vanella, 2014; Consoli and Barbagallo, 2012; Pôças et al., 2015; Rallo and Provenzano, 2013). In this application due to data limitation the daily vegetation indices time series was obtained by linear interpolation between two Landsat acquisitions. This could misrepresent the real vegetative biomass dynamic, thus the temporal change of the transpiration mass and the fractional cover, mainly when the time gap between two cloud-free acquisitions is long. However, the good performance of the $ET_{c\ act,j}$ construction approach particularly in the period of low vegetation cover after the bud break where the evaporative component prevailed suggests that the Landsat derived and interpolated vegetation indices were able to simulate the transpiration mass, canopy water interception and evaporative surface. Furthermore, the current presence of diverse spaceborne systems with a higher spatial resolution and lower revisit time can better represent the vegetation dynamics even if the vegetation dynamics between two acquisitions is still retrieved by linear interpolation. Platforms such as the Sentinels 2 can capture the 5 days vegetation changes in cloud free conditions at a relatively high spatial resolution (10 m).

An additional analysis was performed to separate the effect of SEBAL $ET_{a\ eb}$ estimation errors on the performance of the $ET_{c\ act,j}$ construction procedure. The model was executed by substituting the $ET_{a.eb}$ by the observed $ET_{c\ act\ EC}$ data in the selected Landsat acquisition days. In this way, errors in the constructed $ET_{c\ act,j}$ can be attributed to the model structure, keeping in mind observed SEB closure uncertainties. Using the observed EC data instead of $ET_{a\ eb.}$ yielded a performance (R^2 =0.72, MAE=0.56 mm d^{-1}, RMSE=0.78 mm d^{-1}) in average comparable to that reported in Fig. 5. This analysis may indicate that both SEBAL model estimation errors and SEB closure errors in the considered acquisition days had a similar weight on the performance of the integrated construction procedure.

In addition to the statistical performance metrics documented in Fig. 5, and in aims to further analyze the performance of the integrated $ET_{c\ act}$ construction model, the temporal dynamics of $ET_{c.act,j}$ and $ET_{c\ act\ EC}$ are plotted in Fig. 6a. The proposed procedure reproduced efficiently

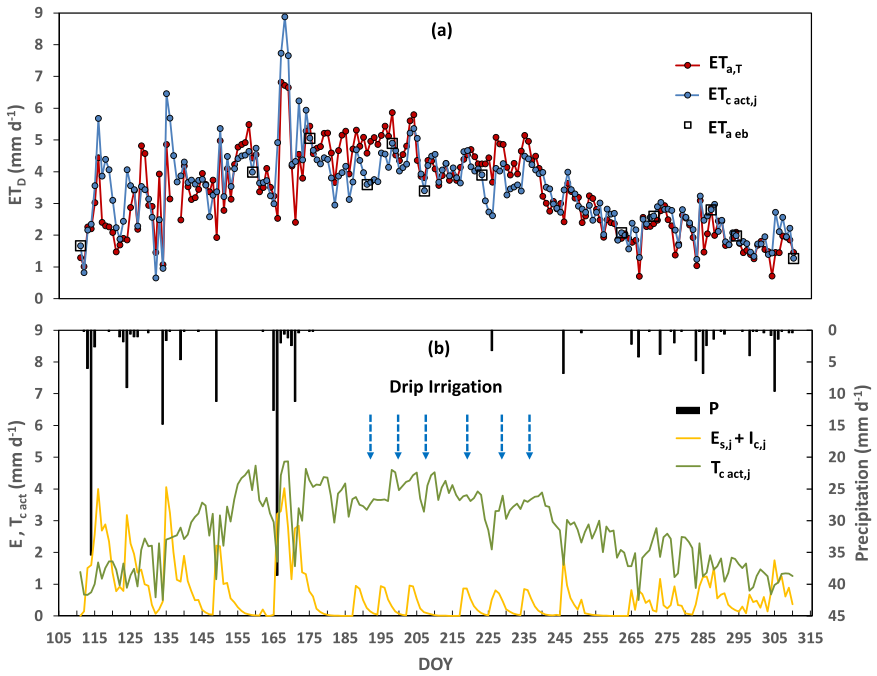

Fig. 6. (a) Daily time series of observed ($ET_{c\ act\ EC}$) and constructed actual evapotranspiration ($ET_{c\ act,j}$), with the indication of the SEBAL estimated $ET_{a\ eb}$ (b) daily dynamics of modeled soil evaporation ($E_{s,j}$), canopy water Interception ($I_{c,j}$) and plant transpiration ($T_{c\ act,j}$), and observed precipitation (P).

the general $ET_{c\ act\ EC}$ trend. The modeled and observed actual ET show similar patterns of monthly and daily variability. The integrated approach allowed adequately simulating actual ET under contrasting dry and wet conditions. Once again, the best performance was obtained from late July to November, where Marras et al. (2016) observed the better energy balance closure for the EC data. The worst performance was noticed in the early summer (from DOY 175–198) due to the SEBAL underestimation of the observed $ET_{c\ act\ EC}$ on DOY 191. However, the average error (less than 20%) was still in the range of accuracy of typical eddy covariance installations (15–30%) (Allen et al., 2011). The performance was also satisfactory from April to June (from DOY 111–175, Fig. 6a). As expected in the early spring period due to the low crop cover, the model demonstrated the significant weight of soil water evaporation in the evapotranspiration process. Still, successively the transpiration component prevailed due to the crop cover establishment (Fig. 6b). In addition to the increase of the atmospheric water demand in the period April-July, from about 3–6 mm d^{-1}, the main driver of the increased transpiration fluxes was the vineyard biomass accumulation. In this period Landsat-derived NDVI augmented from 0.18 to 0.51 and the f_c from 0.09 to 0.5 in agreement with the trend of on-field observed LAI that increased from 0.3 to 2.5 (Marras et al., 2016). This highlighted the importance of considering vegetation changes in modelling $ET_{c\ act}$, especially in crops like vines subjected to major changes during the growth cycle. In the irrigation period the model simulated significant transpiration values supported by adequate soil water availability and small evaporation peaks resulting from local irrigation interventions. The low soil water evaporation was a result of the small wetted soil surface in drip irrigation and the lower energy available at the soil surface due to the higher fractional cover. Successively the transpiration component declined, due to the decrease of atmospheric demand and a slight soil water deficit ($\theta < 0.22$, Fig. 2) which was simulated as a moderate plant stress in the $ET_{c\ act}$ construction approach. As seen in Fig. 6b, the evaporation model showed notable sensitivity to superficial soil moisture changes due to precipitation and irrigation. The distinguished performance of the integrated $ET_{c\ act}$ construction approach during the rainy spring period, when evaporative fluxes are significant and vegetation coverage is low, supported the importance of integrating a soil water evaporation model in the construction procedure.

In construction approaches, $ET_{c\ act}$ is usually estimated as the product of a scaling factor that must be easy to measure or to estimate every day and to which $ET_{c\ act}$ is largely proportional or positively correlated. To show the added value of the proposed integrated $ET_{c\ act}$ construction approach to the forward construction using the referenced ET fraction (ET_{rF}) method that considers only meteorological variations, we compare in Fig. 7 and Table 2 the observed monthly cumulated $ET_{c\ act\ EC}$ values with the simulated $ET_{c\ act,j}$ and those obtained by the referenced ET fraction ($ET_{c\ act\ rF}$). The proposed method yielded good monthly cumulated $ET_{c\ act}$ estimations with errors less than ± 15% in all considered months. It over-performed the referenced ET fraction (ET_{rF}) method, particularly in May and June where biomass changes and soil water evaporation have a significant weight in governing the ET process, knowing that no soil moisture deficit occurred in this period. Instead, from July to October the monthly performance of the simulated $ET_{c\ act,j}$ and $ET_{c\ act\ rF}$ were similar since the crop actual evapotranspiration changes were more governed by the variations of the atmospheric ET demand. This factor is accounted for in the ET_{rF} method, knowing that the vines were not subjected to substantial water stress in this period. Overall, the model showed a better performance in simulating daily $ET_{c\ act}$ values as indicated by the lower MAE and RMSE (Table 2).

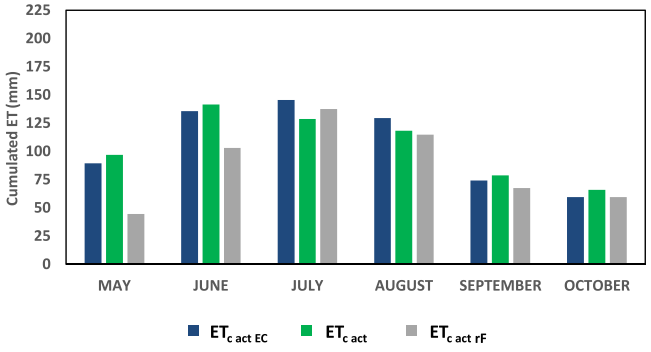

Fig. 7. Monthly cumulated values observed actual evapotraspiration ($ET_{c\ act\ EC}$) compared to crop actual evapotranspiration constructed by the integrated procedure ($ET_{c\ act,}$) and the referenced ET fraction method ($ET_{c\ act\ rF}$).

Table 2
Monthly and all studied period performance of the proposed integrated $ET_{c\ act}$ construction approach and the referenced ET fraction method ($ET_{c\ act\ rF}$).

	MAY	JUNE	JULY	AUGUST	SEPTEMBER	OCTOBER	All period
MAE $ET_{c\ act}$ (mm d^{-1})	0.71	0.67	0.66	0.54	0.29	0.26	0.54
RMSE $ET_{c\ act}$ (mm d^{-1})	0.97	0.89	0.76	0.67	0.37	0.38	0.73
% Difference	8.44	4.27	-11.59	-8.7	6.17	10.81	1.1
MAE $ET_{c\ act\ rF}$ (mm d^{-1})	1.45	1.19	0.62	0.81	0.34	0.23	0.78
RMSE $ET_{c\ act\ rF}$ (mm d^{-1})	1.67	1.53	0.76	0.97	0.43	0.31	1.08
% Difference	-50.21	-24.05	-5.47	-11.3	-9.24	-0.04	-18

4.3. The sensitivity of the integrated daily $ET_{c\ act}$ construction procedure to TIR image availability

The proposed $ET_{c\ act,j}$ construction approach benefits from the relatively high availability of clear-sky image acquisitions. Nevertheless, frequent cloudy sky conditions may hinder an adequate satellite image collection. As an example, in our application the $ET_{a\ eb.}$ estimated by SEBAL on the 21 April 2010 was propagated forwardly for a month and a half due to the absence of clear-sky Landsat images till the date of 8 June 2010. In this section we evaluate how the $ET_{c\ act,j}$ construction model performs to the temporal availability of SEBAL-retrieved $ET_{a\ eb}$. To do this, we hypothesized the worst case, that only one clear-sky image is available to be processed by SEBAL for the entire study period. The real limitation to be assessed is the presence of cloud-free TIR data required by the SEB models, although the upcoming capability of RS systems to capture rapid changes in the TIR domain is promising. An example is the already operating ECOSTRESS sensor that will provide a foundation for the proposed Hyperspectral Infrared Imager (HyspIRI) mission, with a five-day revisit (Lee et al., 2015; Guillevic et al., 2019), the Copernicus Land Surface Temperature Monitoring (LSTM) that will have a spatial resolution of 30–50 m and a temporal resolution lower than three days (Koetz et al., 2018), and the French Space Agency (CNES) and the Indian Space Research Organization (ISRO) TRISHNA satellite mission that will combine high TIR spatial resolution (50 m) and high revisit capacities of two to three days (Lagouarde et al., 2018). Moreover, in addition to Landsat 8, the recent launch (September 2021) of Landsat 9 with the TIRS-2 and OLI-2 instruments aboard will increase the temporal coverage of both VSWIR and TIR data.

In this sensitivity analysis the NDVI dynamics is still represented by the values interpolated between Landsat image acquisitions. The $ET_{a\ eb}$ obtained by SEBAL in the acquisition days reported in Table 1 are used within the proposed $ET_{c\ act,j}$ construction model one at a time to obtain the complete time series of daily $ET_{c\ act,j}$. The $ET_{a\ eb}$ acquired on 21 April was used to forward construct $ET_{c\ act,j}$ till the 6th of November. The $ET_{a\ eb}$ values in other dates were used for both the forward and backward construction of $ET_{c\ act,j}$ between the 21st of April and the 6th of November. These applications allowed to obtain modeled $ET_{c\ act,j}$ time series homogeneous in length. Table 3 and Fig. 8 reports the results of the applied sensitivity analysis. The predicted pattern of the daily and cumulated $ET_{c\ act,j}$ values were evaluated compared to the observed $ET_{c\ act\ EC}$ data. On average, the construction procedure reproduced efficiently the observed daily and cumulated $ET_{c\ act\ EC}$ data. The absolute error in the modeled cumulated $ET_{c\ act}$ did not exceed the 17% of final observed value, except for the backward $ET_{c\ act}$ construction using the $ET_{a\ eb}$ of 6-Nov. The best performance was obtained when the summer values of $ET_{a\ eb}$ were used for $ET_{c\ act,j}$ construction. The worst performance was obtained for 21-Apr and 6-Nov where there was a low evapotranspiration. This suggested that low values of $ET_{a\ eb}$ such as those obtained in wet spring and autumn should be used with caution for the $ET_{c\ act}$ series construction over long period (months). Overall, the sensitivity analysis results suggest that the integrated proposed approach could simulate $ET_{c\ act}$ even in scarce data conditions. This integrated modelling approach can sustain and/or reduce the need for low revisit intervals of high spatial resolution satellite based TIR, knowing that an adequate VSWIR and TIR satellite image collections for $ET_{c\ act}$ estimation can still be hindered by frequent cloudy sky conditions. Although, low revisit time systems may provide a significant improvement in temporal sampling to monitor $ET_{c\ act}$, an integrated modelling approach is still required to properly simulate the rapid dynamics of soil-plant-atmosphere continuum that can be missed even with revisit time of few days in cloud free conditions particularly in intensive irrigated agriculture. Indeed, Delogu et al. (2021) considered that the future tendency to produce robust $ET_{c\ act}$ estimates at plot scale will probably rely not only on remote sensing data acquired at different wavelengths and/or resolutions, but also on their combination with local water balance models constrained at regular intervals by $ET_{a\ eb}$ estimates from the TIR domain.

Table 3
Cumulated actual evapotranspiration values and performance obtained by using one at a time the $ET_{a\ eb}$ value for the construction of $ET_{c\ act}$ from 21-April to 6 November 2010. *With respect to the observed cumulated $ET_{c\ act\ EC}$ (667 mm) of the studied period.

Acquisition day (A.D.)	Cumulated $ET_{c\ act}$ % difference*	R^2	MAE (mm)	RMSE (mm)
All data	1.1%	0.71	0.54	0.73
21-Apr	17%	0.78	0.73	0.90
8-June	1.8%	0.73	0.51	0.70
24-June	-11%	0.66	0.69	0.86
10-July	-8.7%	0.68	0.63	0.81
17-July	-1,8%	0.71	0.53	0.72
26-July	4.4%	0.74	0.51	0.71
11-Aug	2.2%	0.73	0.51	0.70
19-Sept	-15%	0.63	0.78	0.96
28-Sept	-2.4%	0.73	0.51	0.70
14-Oct	-2.7%	0.71	0.54	0.73
21-Oct	-3.6%	0.70	0.55	0.74
6-Nov	-25%	0.55	1.04	1.23

5. Conclusions

The paper presented a simple but effective procedure to construct continuous time series of actual evapotranspiration starting from infrequent estimations of $ET_{a\ eb}$ obtained by a SEB model applied on Landsat satellite data. The proposed approach integrated two widely used models, the SEBAL for the retrieval of $ET_{a\ eb}$ on image acquisition days and the FAO-56 model to estimate daily soil water evaporation. The daily $ET_{c\ act}$ construction approach propagates over time the actual crop transpiration obtained on the satellite image acquisition days by using remotely sensed NDVI and on-field measurements of potential evapotranspiration and soil moisture. The integrated daily $ET_{c\ act}$ construction procedure reproduced efficiently the observed daily values of $ET_{c\ act\ EC}$ during the complete vegetative annual cycle of a vineyard with partial soil coverage. The temporal analysis of the modeled daily ET datastream emphasized the importance of integrating the vegetative biomass dynamics and a soil water evaporation model in the daily $ET_{c\ act}$ construction approach. Considering the vegetation dynamics through NDVI increase in late spring allowed to account for the rise in the grapevine's transpiration due to the development of the plant green biomass. Furthermore, the evaporation model was fundamental for reproducing the evaporation peaks after significant rain events, particularly in the early spring period with low soil coverage. Nevertheless,

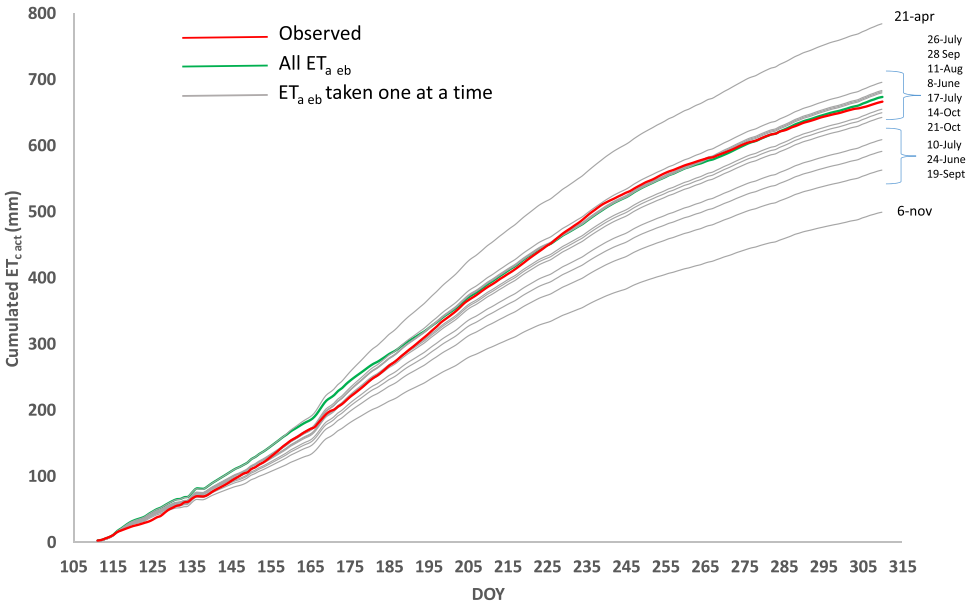

Fig. 8. Cumulated values of observed actual evapotraspiration ($ET_{c\ act\ EC}$, red line), of $ET_{c\ act}$ simulated using the complete $ET_{a\ eb}$ dataset (green line), and the ones simulated using a single acquisition day $ET_{a\ eb}$ (grey lines).

further testing of the evaporation model should be performed. A cumulative monthly comparison with the referenced ET fraction (ET_{rF}) method showed the lead of the proposed approach particularly when biomass changes and soil water evaporation have a significant weight in governing the ET process. The inclusion of a stress coefficient is required for considering the variation of plant transpiration due to soil moisture changes between acquisition days. Soil moisture data indicated that the studied vineyard suffered of mild water limitation for a short period in late summer, which didn't permit a profound analysis of the effect of plant water stress on transpiration. More investigation with diverse dataset is needed to evaluate the effectiveness of the plant stress correction term in constructing of the transpiration time series.

The proposed construction approach is well suited for the near real-time modelling of daily $ET_{c\ act}$, which is of great importance in water management and irrigation scheduling. Although in this application the used Landsat NDVI data permits only a historical analysis, nowadays several available free or low-cost satellite platforms can provide NDVI scenes with a range of few days (e.g., Sentinels 2) supporting the near real-time monitoring of vegetation dynamics. Moreover, this approach can benefit from low revisit time and high spatial resolution systems (e.g., ECOSTRESS) that may provide a significant improvement in temporal sampling to monitor $ET_{c\ act}$ on plot scale. Nevertheless, results also shown that integrating a local water balance modelling approach that accounts to soil properties and simulate the dynamics in the soil-vegetation-atmosphere transfer system can significantly reduce the need of temporal TIR data.

Here, soil moisture was directly observed in the field. For applications over a larger scale, this approach can be supported by the current availability of low-cost soil probes. Differently, spatialized pixel surface soil moisture dynamics over large areas can be derived by physically-based models using optical, microwave, synthetic aperture radar, or TIR remote sensing data, even though the application of these methods both on field scale and on daily bases is still a matter of research. Alternatively, soil moisture dynamics in the root zone can be estimated by hydrological modeling approaches, for example by using the transient flow Richards equation. The current and future development of diverse spaceborne remote sensing platforms able of acquiring data at different wavelengths and/or resolutions will definitely improve $ET_{c\ act}$ estimates at plot scale. However, a robust $ET_{c\ act}$ estimation will also rely on their combination with local water balance models. The application of data assimilation, fusion techniques and integrating the proposed $ET_{c\ act}$ construction procedure with the soil water balance modeling is an objective we intend to realize in the near future.

CRediT authorship contribution statement

H.A. and M.P. developed the hydrological analysis. S.M. and S.C. acquired and provided the field data that were processed by H.A., M.P., S.P. and F.G.; M.P. and D.S. coordinated the team and supervised the research. All the authors analyzed the results and contributed to write and to revise the manuscript.

Declaration of Competing Interest

The authors declare that they have no known competing financial interests or personal relationships that could have appeared to influence the work reported in this paper.

Acknowledgments

This research was developed in the framework of the *HYDROSARD* project funded by the Regione Autonoma Sardegna and was carried out at the Department of Agriculture Sciences of the University of Sassari. The Authors would like to thank Argiolas Company for hospitality. The authors would also like to acknowledge the University of Sassari 2020 research fund FAR2019SPANO, FAR2020SIRCACB, FAR2019PIRASTRU and FAR2020PIRASTRUMA.

References

Ahmad, M.-D., Bastiaanssen, W.G.M., Feddes, R.A., 2005. A new technique to estimate net groundwater use across large irrigated areas by combining remote sensing and water balance approaches, Rechna Doab, Pakistan. Hydrogeol. J. 13, 653–664. https://doi.org/10.1007/s10040-004-0394-5.

Ahmad, M.D., Kirby, M., Islam, M.S., Hossain, M.J., Islam, M.M., 2014. Groundwater use for irrigation and its productivity: status and opportunities for crop intensification for food security in Bangladesh. Water Resour. Manag. 28, 1415–1429. https://doi.org/10.1007/s11269-014-0560-z.

Akbari, M., Toomanian, N., Droogers, P., Bastiaanssen, W., Gieske, A., 2007. Monitoring irrigation performance in Esfahan, Iran, using NOAA satellite imagery. Agric. Water Manag. 88 (1–3), 99–109. https://doi.org/10.1016/j.agwat.2006.10.019.

Al Zayed, I.S., Elagib, N.A., Ribbe, L., Heinrich, J., 2015. Spatio-temporal performance of large-scale Gezira irrigation scheme, Sudan. Agric. Syst. 133, 131–142. https://doi.org/10.1016/j.agsy.2014.10.009.

Alfieri, J.G., Anderson, M.C., Kustas, W.P., Cammalleri, C., 2017. Effect of the revisit interval and temporal upscaling methods on the accuracy of remotely sensed evapotranspiration estimates. Hydrol. Earth Syst. Sci. 21 (1), 83–98.
Allen, R.G., Pereira, L.S., Howell, T.A., Jensen, M.E., 2011. Evapotranspiration information reporting: I. Factors governing measurement accuracy. Agric. Water Manag. 98 (6), 899–920.
Allen, R.G., Tasumi, M., Trezza, R., 2007. Satellite-based energy balance for mapping evapotranspiration with internalized calibration (METRIC)—Model. J. Irrig. Drain. Eng. 133 (4), 380–394.
Allen, R.G., Pereira, L.S., Raes, D., Smith, M. (1998). Crop evapotranspiration: Guidelines for computing crop water requirements. Irr. Drain. Paper 56. UN-FAO, Rome.
Awada, H., Ciraolo, G., Maltese, A., Provenzano, G., Hidalgo, M.A.M., Còrcoles, J.I., 2019. Assessing the performance of a large-scale irrigation system by estimations of actual evapotranspiration obtained by Landsat satellite images resampled with cubic convolution. Int. J. Appl. Earth Obs. Geoinf. 75, 96–105. https://doi.org/10.1016/j.jag.2018.10.016.
Awada, H., Di Prima, S., Sirca, C., Giadrossich, F., Marras, S., Spano, D., Pirastru, M., 2021. Daily actual evapotranspiration estimation in a mediterranean ecosystem from landsat observations using SEBAL approach. Forests 12 (2), 189.
Bastiaanssen, W.G.M., 2000. SEBAL-based sensible and latent heat fluxes in the irrigated Gediz Basin, Turkey. J. Hydrol. 229, 87–100. https://doi.org/10.1016/S0022-1694(99)00202-4.
Bastiaanssen, W.G.M., Ahmad, M.U.D., Chemin, Y., 2002. Satellite surveillance of evaporative depletion across the Indus Basin. Water Resour. Res. 38 (12), 9–1–9–9, 9-1.
Bastiaanssen, W.G.M., Brito, R.A.L., Bos, M.G., Souza, R.A., Cavalcanti, E.B., Bakker, M. M., 2001. Low cost satellite data for monthly irrigation performance monitoring: benchmarks from Nilo Coelho, Brazil. Irrig. Drain. Syst. 15 (1), 53–79.
Bastiaanssen, W.G.M., Noordman, E.J.M., Pelgrum, H., Davids, G., Thoreson, B.P., Allen, R.G., 2005. SEBAL model with remotely sensed data to improve water-resources management under actual field conditions, 2005 J. Irrig. Drain. Eng. 131, 85–93. https://doi.org/10.1061/(ASCE)0733-9437,131:1(85).
Bastiaanssen, W.G.M., Menenti, M., Feddes, R.A., Holtslag, A.A.M., 1998a. A remote sensing surface energy balance algorithm for land (SEBAL): 1. Formul. Hydrol. 212–213 (1998), 198–212.
Bastiaanssen, W.G.M.; Pelgrum, H.; Soppe, R.W.O.; Allen, R.G.; Thoreson, B.P.; de C. Teixeira, A.H. (2008). Thermal-Infrared Technology for Local and Regional Scale Irrigation Analyses in Horticultural Systems. In Proceedings of the Acta Horticulturae, Leuven, Belgium, 30 June; International Society for Horticultural Science (ISHS); pp. 33–46, Mildura, Australia.
Bastiaanssen, W.G.M., Pelgrum, H., Wang, J., Ma, Y., Moreno, J.F., Roerink, G.J., Van der Wal, T., 1998b. A remote sensing surface energy balance algorithm for land (SEBAL): part 2: validation. J. Hydrol. 212, 213–229. https://doi.org/10.1016/S0022-1694(98)00254-6.
Bastiaanssen, W.G.M., Van der Wal, T., Visser, T.N.M., 1996. Diagnosis of regional evaporation by remote sensing to support irrigation performance assessment. Irrig. Drain. Syst. 10 (1), 1–23.
Beeri, O., Pelta, R., Shilo, T., Mey-Tal, S., Tanny, J., 2019. Accuracy of crop coefficient estimation methods based on satellite imagery. Precis. Agric. 19 (9), 437–444.
Bhattarai, N., Dougherty, M., Marzen, L.J., Kalin, L., 2012. Validation of evaporation estimates from a modified surface energy balance algorithm for land (SEBAL) model in the south-eastern United States. Remote Sens. Lett. 3 (6), 511–519.
Bhattarai, N., Shaw, S.B., Quackenbush, L.J., Im, J., Niraula, R., 2016. Evaluating five remote sensing based single-source surface energy balance models for estimating daily evapotranspiration in a humid subtropical climate. Int. J. Appl. Earth Obs. Geoinf. 49, 75–86.
Bhattarai, N., Quackenbush, L.J., Dougherty, M., Marzen, L.J., 2014. A simple Landsat–MODIS fusion approach for monitoring seasonal evapotranspiration at 30 m spatial resolution. Int. J. Remote. Sens. 36, 115–143.
Bindhu, V.M., Narasimhan, B., Sudheer, K.P., 2013. Development and verification of a non-linear disaggregation method (NL-DisTrad) to downscale MODIS land surface temperature to the spatial scale of Landsat thermal data to estimate evapotranspiration. Remote Sens. Environ. 135, 118–129.
Bisquert, M., Sánchez, J.M., López-Urrea, R., Caselles, V., 2016. Estimating high resolution evapotranspiration from disaggregated thermal images. Remote Sens. Environ. 187, 423–433.
Blatchford, M.L., Karimi, P., Bastiaanssen, W.G.M., Nouri, H., 2018. From global goals to local gains—A framework for crop water productivity. ISPRS Int. J. Geo-Inf. 7 (11), 414. https://doi.org/10.3390/ijgi7110414.
Brutsaert, W., Sugita, M., 1992. Application of self-preservation in the diurnal evolution of the surface energy budget to determine daily evaporation. J. Geophys. Res. Atmos. 97, 18377–18382. https://doi.org/10.1029/92JD00255.
Cammalleri, C., Anderson, M.C., Gao, F., Hain, C.R., Kustas, W.P., 2013. A data fusion approach for mapping daily evapotranspiration at field scale. Water Resour. Res. 49 (8), 4672–4686.
Cammalleri, C., Agnese, C., Ciraolo, G., Minacapilli, M., Provenzano, G., Rallo, G., 2010. Actual evapotranspiration assessment by means of a coupled energy/hydrologic balance model: validation over an olive grove by means of scintillometry and measurements of soil water contents. J. Hydrol. 392, 70–82. https://doi.org/10.1016/j.jhydrol.2010.07.046.
Cammalleri, C., Anderson, M.C., Ciraolo, G., D'Urso, G., Kustas, W.P., La Loggia, G., Minacapilli, M., 2012. Applications of a remote sensing-based two-source energy balance algorithm for mapping surface fluxes without in situ air temperature observations. Remote Sens. Environ. 124, 502–515. https://doi.org/10.1016/j.rse.2012.06.009.
Campos, I., Neale, C.M.U., Calera, A., Balbontin, C., González-Piqueras, J., 2010. Assessing satellite-based basal crop coefficients for irrigated grapes (Vitis vinifera L.). Agric. Water Manag. 97, 1760–1768.
Carrasco-Benavides, M., Ortega-Farías, S., Lagos, L.O., Kleissl, J., Morales, L., Poblete-Echeverría, C., Allen, R.G., 2012. Crop coefficients and actual evapotranspiration of a drip-irrigated Merlot vineyard using multispectral satellite images. Irrig. Sci. 30 (6), 485–497.
Chávez, J.L., Neale, C.M.U., Prueger, J.H., Kustas, W.P., 2008. Daily evapotranspiration estimates from extrapolating instantaneous airborne remote sensing ET values. Irrig. Sci. 27, 67–81. https://doi.org/10.1007/s00271-008-0122-3.
Choudhury, B.J., 1987. Relationships between vegetation indices, radiation absorption, and net photosynthesis evaluated by a sensitivity analysis. Remote Sens. Environ. 22 (2), 209–233.
Consoli, S., Vanella, D., 2014. Mapping crop evapotranspiration by integrating vegetation indices into a soil water balance model. Agric. Water Manag. 143, 71–81.
Consoli, S., Barbagallo, S., 2012. Estimating water requirements of an irrigated mediterranean vineyard using a satellite-based approach. J. Irrig. Drain. Eng. 138 (10), 896–904.
Crago, R.D., 1996. Conservation and variability of the evaporative fraction during the daytime. J. Hydrol. 180, 173–194. https://doi.org/10.1016/0022-1694(95)02903-6.
D'Urso, G., 2001. Simulation and Management of On-Demand Irrigation Systems: A Combined Agro-hydrological Approach (PhD Dissertation). Wageningen University, p. 174 (PhD Dissertation).
Delogu, E., Olioso, A., Alliès, A., Demarty, J., Boulet, G., 2021. Evaluation of multiple methods for the production of continuous evapotranspiration estimates from TIR remote sensing. Remote Sens. 13 (6), 1086.
De Vries, D.A. (1963). Thermal properties of soils. In W.R. van Wijk (Ed.), Physics of Plant Environment, North-Holland, Amsterdam, pp. 210–235.
Dickinson, R.E., Henderson-Sellers, A., Rosenzweig, C., Sellers, P.J., 1991. Evapotranspiration models with canopy resistance for use in climate models, a review. Agric. For. Meteorol. 54 (2–4), 373–388.
Droogers, P., Bastiaanssen, W.G., Beyazgül, M., Kayam, Y., Kite, G.W., Murray-Rust, H., 2000. Distributed agro-hydrological modeling of an irrigation system in western Turkey. Agric. Water Manag. 43 (2), 183–202.
Droogers, P., Bastiaanssen, W., 2002. Irrigation performance using hydrological and remote sensing modeling. J. Irrig. Drain. Eng. 2002 (128), 11–18. https://doi.org/10.1061/(ASCE)0733-9437128:1(11).
Elhaddad, A., Garcia, L.A., 2008. Surface energy balance-based model for estimating evapotranspiration taking into account spatial variability in weather. J. Irrig. Drain. Eng. 134, 681–689. https://doi.org/10.1061/(ASCE)0733-9437(2008)134:6(681).
Er-Raki, S., Rodriguez, J.C., Garatuza-Payan, J., Watts, C.J., Chehbouni, A., 2013. Determination of crop evapotranspiration of table grapes in a semi-arid region of Northwest Mexico using multi-spectral vegetation index. Agric. Water Manag. 122, 12–19.
Fernandes De Oliveira, A., Mameli, M.G., De Pau, L., Satta, D., Nieddu, G. (2013). Deficit irrigation strategies in Vermentino for improving groundwater use in clay soil. In: Proceedings of the 18th International Symposium of the Group of International Experts of vitivinicultural System for CoOperation (GiESCO 2013) (pp. 134–139).
Gao, F., Masek, J., Schwaller, M., Hall, F., 2006. On the blending of the Landsat and MODIS surface reflectance: Predicting daily Landsat surface reflectance. IEEE Trans. Geosci. Remote Sens. 44 (8), 2207–2218.
Galleguillos, M., Jacob, F., Prévot, L., French, A., Lagacherie, P., 2011. Comparison of two temperature differencing methods to estimate daily evapotranspiration over a Mediterranean vineyard watershed from ASTER data. Remote Sens. Environ. 115 (6), 1326–1340.
Gowda, P.H., Chávez, J.L., Howell, T.A., Marek, T.H., New, L.L., 2008. Surface energy balancebased evapotranspiration mapping in the Texas high plains. Sensors 8 (8), 5186–5201.
Guillevic, P.C., Olioso, A., Hook, S.J., Fisher, J.B., Lagouarde, J.P., Vermote, E.F., 2019. Impact of the revisit of thermal infrared remote sensing observations on evapotranspiration uncertainty—A sensitivity study using AmeriFlux Data. Remote Sens. 11 (5), 573.
Gutman, G., Ignatov, A., 1998. The derivation of the green vegetation fraction from NOAA/AVHRR data for use in numerical weather prediction models. Int. J. Remote Sens. 19 (8), 1533–1543.
Häusler, M., Conceição, N., Tezza, L., Sánchez, J.M., Campagnolo, M.L., Häusler, A.J., Silva, J.M., Warneke, T., Heygster, G., Ferreira, M.I., 2018. Estimation and partitioning of actual daily evapotranspiration at an intensive olive grove using the STSEB model based on remote sensing. Agric. Water Manag. 201, 188–198.
Immerzeel, W.W., Droogers, P., 2008. Calibration of a distributed hydrological model based on satellite evapotranspiration. J. Hydrol. 349, 411–424. https://doi.org/10.1016/j.jhydrol.2007.11.017.
Jarvis, N.J., 1989. A simple empirical model of root water uptake. J. Hydrol. 107 (1–4), 57–72.
Knipper, K.R., Kustas, W.P., Anderson, M.C., Alfieri, J.G., Prueger, J.H., Hain, C.R., Gao, F., Yang, Y., McKee, L.G., Nieto, H., Hipps, L.E., Alsina, M.M., Sanchez, L., 2019. Evapotranspiration estimates derived using thermal-based satellite remote sensing and data fusion for irrigation management in California vineyards. Irrig. Sci. 37 (3), 431–449.
Koetz, B., Bastiaanssen, W., Berger, M., Defourney, P., Del Bello, U., Drusch, M., Drinkwater, M., Duca, R., Fernandez, V., Ghent, D., Guzinski, R., Hoogeveen, J., Hook, S., Lagouarde, J., Lemoine, G., Manolis, I., Martimort, P., Masek, J., Massart, M., Notarnicola, C., Sobrino, J., & Udelhoven, T. (2018, July). High spatio-temporal resolution land surface temperature mission-a copernicus candidate mission in

support of agricultural monitoring. In: Proceedings of the IGARSS 2018–2018 IEEE International Geoscience and Remote Sensing Symposium (pp. 8160–8162). IEEE.
Kustas, W.P., Norman, J.M., Anderson, M.C., French, A.N., 2003. Estimating subpixel surface temperatures and energy fluxes from the vegetation index-radiometric temperature relationship. Remote Sens. Environ. 85, 429–440.
Lagouarde, J.P., Bhattacharya, B.K., Crebassol, P., Gamet, P., Babu, S.S., Boulet, G., Briottet, X., Buddhiraju, K.M., Cherchali, S., Dadou, I., Dedieu, G., Gouhier, M., Hagolle, O., Irvine, M., Jacob, F., Kumar, A., Kumar, K.K., Laignel, B., Mallick, K., Murthy, C.S., Olioso, A., Ottlé, C., Pandya, M.R., Raju, P.V., Roujean, J., Sekhar, M., Shukla, M.V., Singh, S.K., Sobrino, J., Ramakrishnan, R. (2018). The Indian-French Trishna mission: Earth observation in the thermal infrared with high spatio-temporal resolution. In: Proceedings of the IGARSS 2018–2018 IEEE International Geoscience and Remote Sensing Symposium (pp. 4078–4081). IEEE.
Lee, C.M., Cable, M.L., Hook, S.J., Green, R.O., Ustin, S.L., Mandl, D.J., Middleton, E.M., 2015. An introduction to the NASA Hyperspectral InfraRed Imager (HyspIRI) mission and preparatory activities. Remote Sens. Environ. 167, 6–19.
Li, S., Zhao, W., 2010. Satellite-based actual evapotranspiration estimation in the middle reach of the Heihe River Basin using the SEBAL method. Hydrol. Process. 24 (23), 3337–3344.
Ma, Y., Liu, S., Song, L., Xu, Z., Liu, Y., Xu, T., Zhu, Z., 2018. Estimation of daily evapotranspiration and irrigation water efficiency at a Landsat-like scale for an arid irrigation area using multi-source remote sensing data. Remote Sens. Environ. 216, 715–734.
Maltese, A., Awada, H., Capodici, F., Ciraolo, G., La Loggia, G., Rallo, G., 2018. On the use of the eddy covariance latent heat flux and sap flow transpiration for the validation of a surface energy balance model. Remote Sens. 10 (2), 195.
Maltese, A.; Capodici, F.; Ciraolo, G.; Loggia, G.L.; Rallo, G. (2013). Assessing Daily Actual Evapotranspiration through Energy Balance: An Experiment to Evaluate the Selfpreservation Hypothesis with Acquisition Time. In: Proceedings of the Remote Sensing for Agriculture, Ecosystems, and Hydrology XV, Dresden, Germany, 16 October 2013; International Society for Optics and Photonics; Volume 8887, p. 888718.
Mameli, M.G., De Pau, L., Satta, D., Ventroni, G., Zurru, R. (2012). Study of the effects of different irrigation scheduling on some vegetative and productive characteristics of'Vermentino'. In: Proceedings of the *VII International Symposium on Irrigation of Horticultural Crops* 1038 (pp. 545–552).
Marras, S., Achenza, F., Snyder, R.L., Duce, P., Spano, D., Sirca, C., 2016. Using energy balance data for assessing evapotranspiration and crop coefficients in a Mediterranean vineyard. Irrig. Sci. 34 (5), 397–408.
Masia, S., Trabucco, A., Spano, D., Snyder, R.L., Sušnik, J., Marras, S., 2021. A modelling platform for climate change impact on local and regional crop water requirements. Agric. Water Manag. 255, 107005.
McCabe, M.F., Wood, E.F., 2006. Scale influences on the remote estimation of evapotranspiration using multiple satellite sensors. Remote Sens. Environ. 105 (4), 271–285.
Menenti, M., 2000. Evaporation in Remote sensing in hydrology and water management. Springer, Berlin, Heidelberg, pp. 157–196.
Minacapilli, M., Cammalleri, C., Ciraolo, G., Rallo, G., Provenzano, G., 2016. Using scintillometry to assess reference evapotranspiration methods and their impact on the water balance of olive groves. Agric. Water Manag. 170, 49–60.
Minacapilli, M., Agnese, C., Blanda, F., Cammalleri, C., Ciraolo, G., D'Urso, G., Iovino, M., Pumo, D., Provenzano, G., Rallo, G., 2009. Estimation of actual evapotranspiration of mediterranean perennial crops by means of remote-sensing based surface energy balance models. Hydrol. Earth Syst. Sci. 13, 1061–1074. https://doi.org/10.5194/hess-13-1061-2009.
Molden, D., Sakthivadivel, R., 1999. Water accounting to assess use and productivity of water. Int. J. Water Resour. Dev. 15 (1–2), 55–71. https://doi.org/10.1080/07900629948934.
Molden, D., Oweis, T., Steduto, P., Bindraban, P., Hanjra, M.A., Kijne, J., 2010. Improving agricultural water productivity: Between optimism and caution. Agric. Water Manag. 97 (4), 528–535.
Morse, A., Tasumi, M., Allen, R.G., Kramber, W.J. (2000). Application of the SEBAL methodology for estimating consumptive use of water and streamflow depletion in the Bear River Basin of Idaho through remote sensing. Final report submitted for publication to the Raytheon Systems Company, Earth Observation System Data and Information System Project, by Idaho Department of Water Resources and University of Idaho.
Muthuwatta, L.P., Ahmad, M.-D., Bos, M.G., Rientjes, T.H.M., 2010. Assessment of water availability and consumption in the Karkheh River Basin, Iran—Using remote sensing and geo-Statistics. Water Resour. Manag. 24, 459–484. https://doi.org/10.1007/s11269-009-9455-9.
Norman, J.M., Kustas, W.P., Humes, K.S., 1995. Source approach for estimating soil and vegetation energy fluxes in observations of directional radiometric surface temperature. Agric. For. Meteorol. 77 (3–4), 263–293.
Ochoa-Sánchez, A., Crespo, P., Carrillo-Rojas, G., Sucozhañay, A., Célleri, R., 2019. Actual evapotranspiration in the high Andean grasslands: a comparison of measurement and estimation methods. Front. Earth Sci. 7, 55.
O'Connell, M.G., Whitfield, D.M., Abuzar, M., Sheffield, K.J., McClymont, L., McAllister, A.T., Tatura, V., 2011. Satellite Remote Sensing of water use and vegetation cover to derive crop coefficients for crops grown in Sunraysia Irrigation Region of Victoria, Australia. Acta Hortic. 889, 543–549.
Olivera-Guerra, L., Mattar, C., Merlin, O., Durán-Alarcón, C., Santamaría-Artigas, A., Fuster, R., 2017. An operational method for the disaggregation of land surface temperature to estimate actual evapotranspiration in the arid region of Chile. ISPRS J. Photogramm. Remote Sens. 128, 170–181.
Pôças, I., Paço, T.A., Paredes, P., Cunha, M., Pereira, L.S., 2015. Estimation of actual crop coefficients using remotely sensed vegetation indices and soil water balance modelled data. Remote Sens. 7 (3), 2373–2400.
Prueger, J.H., Hatfield, J.L., Parkin, T.B., Kustas, W.P., Hipps, L.E., Neale, C.M.U., MacPherson, J.I., Eichinger, W.E., Cooper, D.I., 2005. Tower and aircraft eddy covariance measurements of water vapor, energy, and carbon dioxide fluxes during SMACEX. J. Hydrometeors 6, 954–960. https://doi.org/10.1175/JHM457.1.
Rallo, G., Provenzano, G., 2013. Modelling eco-physiological response of table olive trees (Olea europaea L.) to soil water deficit conditions. Agric. Water Manag. 120, 79–88.
Rodell, M., Velicogna, I., Famiglietti, J.S., 2009. Satellite-based estimates of groundwater depletion in India. Nature 460, 999–1002. https://doi.org/10.1038/nature08238.
Rouse, J.W., Haas, R.H., Schell, J.A., Deering, D.W., Harlan, J.C. (1974). Monitoring the vernal advancement and retrogradation (green wave effect) of natural vegetation. NASA/GSFC Type III Final Report, Greenbelt, Maryland, p. 371.
Semmens, K.A., Anderson, M.C., Kustas, W.P., Gao, F., Alfieri, J.G., McKee, L., Prueger, J. H., Hain, C.R., Cammalleri, C., Yang, Y., Xia, T., Sanchez, L., del Mar Alsina, M., Vélez, M., 2016. Monitoring daily evapotranspiration over two California vineyards using Landsat 8 in a multi-sensor data fusion approach. Remote Sens. Environ. 185, 155–170.
Senay, G.B., Schauer, M., Friedrichs, M., Velpuri, N.M., Singh, R.K., 2017. Satellite-based water use dynamics using historical Landsat data (1984–2014) in the southwestern United States. Remote Sens. Environ. 202, 98–112.
Shuttleworth, W.J., Gurney, R.J., Hsu, A.Y., Ormsby, J.P., 1989. FIFE: the variation in energy partitioning at surface flux sites. May 1989. In: Rango, A. (Ed.), Remote Sensing and Large-Scale Processes (Proceedings of the IAHS third international Assembly, vol. 186. IAHS Publication, Baltimore, MD, pp. 67–74. May 1989.
Singh, R.K., Liu, S., Tieszen, L.L., Suyker, A.E., Verma, S.B., 2012. Estimating seasonal evapotranspiration from temporal satellite images. Irrig. Sci. 30 (4), 303–313.
Stanhill, G., 1986. Water use efficiency. Adv. Agron. 39, 53–85.
Su, Z., 2002. The Surface Energy Balance System (SEBS) for estimation of turbulent heat fluxes. Hydrol. Earth Syst. Sci. 6 (1), 85–100.
Timmermans, W.J., Kustas, W.P., Anderson, M.C., French, A.N., 2007. An intercomparison of the surface energy balance algorithm for land (SEBAL) and the two-source energy balance (TSEB) modeling schemes. Remote Sens. Environ. 108 (4), 369–384.
Trezza, R., Allen, R.G., Tasumi, M., 2013. Estimation of actual evapotranspiration along the Middle Rio Grande of New Mexico using MODIS and Landsat imagery with the METRIC model. Remote Sens. 5 (10), 5397–5423.
Trezza, R., Allen, R.G., Kilic, A., Ratcliffe, I., Tasumi, M., 2018. Influence of Landsat revisit frequency on time-integration of evapotranspiration for agricultural water management. Advanced Evapotranspiration Methods and Applications. IntechOpen.
Wagle, P., Bhattarai, N., Gowda, P.H., Kakani, V.G., 2017. Performance of five surface energy balance models for estimating daily evapotranspiration in high biomass sorghum. Isprs J. Photogramm. Remote. Sens. 128, 192–203.
Wilson, K., Goldstein, A., Falge, E., Aubinet, M., Baldocchi, D., Berbigier, P., Bernhofer, C., Ceulemans, R., Dolman, H., Field, C., Grelle, A., Ibrom, A., Law, B.E., Kowalski, A., Meyers, T., Moncrieff, J., Monson, R., Oechel, W., Tenhunen, J., Valentini, R., Verma, S., 2002. Energy balance closure at FLUXNET sites. Agric. For. Meteorol. 113 (1–4), 223–243.
Zwart, S.J., Bastiaanssen, W.G.M., de Fraiture, C., Molden, D.J., 2010. A global benchmark map of water productivity for rainfed and irrigated wheat. Agric. Water Manag 97, 1617–1627. https://doi.org/10.1016/j.agwat.2010.05.018.
Zwart, S.J., Bastiaanssen, W.G.M., 2007. SEBAL for detecting spatial variation of water productivity and scope for improvement in eight irrigated wheat systems. Agric. Water Manag. 89 (3), 287–296.